Deriving rock uplift histories from data-driven inversion of river profiles

Christoph Glotzbach*
Institute of Geology, Leibniz University Hannover, Callinstrasse 30, 30167 Hannover, Germany

ABSTRACT

Reconstructing the evolution of Earth's landscape is a key to understanding its future evolution and to identifying the driving forces that shape Earth's surface. Cosmogenic nuclide and thermochronological investigations are routinely used to quantify Earth surface processes over 10^2–10^4 yr and 10^6–10^7 yr, respectively. A comparison of the rates of surface processes derived from these methods is, however, hampered by the large difference in their time scales. River profiles bridge this time gap and record the regional uplift history over 10^2–10^7 yr. Here I present an integrative inverse modeling approach to simultaneously reconstruct river profiles, model thermochronological and cosmogenic nuclide data, and derive robust information about landscape evolution over thousands to millions of years. An efficient inversion routine is used to solve the forward problem and find the best uplift history and erosional parameters (such as the exponents of discharge [*m*] and slope [*n*] in the stream power equation) that reproduce the observed data. I test the performance of the algorithm by inverting a synthetic data set and a data set from the Sila massif (Italy). Results show that even complicated uplift histories can be reliably retrieved by the combined interpretation of river profiles and thermochronological and cosmogenic nuclide data.

INTRODUCTION

Earth's surface is constantly evolving as a response to changes in its boundary conditions, such as changes in tectonic uplift and climate change (e.g., England and Molnar, 1990). During recent decades, important questions in Earth sciences have emerged from intense research about the coupling between tectonics, climate, and resulting landscape evolution. As such, the potential response of climate to intensified mountain building by CO_2 drawdown via increased chemical weathering is highly debated (e.g., Raymo and Ruddiman, 1992; West, 2012; Maher and Chamberlain, 2014). Analytical methods such as thermochronological tools and cosmogenic nuclide dating are routinely used to quantify Earth surface processes (e.g., Reiners and Ehlers, 2005; von Blanckenburg, 2005). Resulting rates of surface processes are representative over different time scales; e.g., a constant erosion rate of 0.1 mm/yr yields an apatite (U-Th)/He age of ca. 22 Ma (for a steady-state one-dimensional [1-D] thermal model with 500 °C at 30 km depth and 10 °C at the surface) and a ^{10}Be age of ca. 6 ka (assuming an attenuation length of 160 g/cm^2 and a density of 2.7 g/cm^3), respectively. Although these methods can be combined (e.g., Buscher et al., 2013; Glotzbach et al., 2013), estimating virtually continuous rates of landscape evolution across these time scales remains a challenge and was therefore identified as a high-priority research task (National Research Council, 2010).

Inverse models for the interpretation of thermochronological data use, in almost all applications, a simplistic approximation of topographic evolution. The most widely applicable program, Pecube, is flexible in incorporating changes in topography (e.g., Braun et al., 2012), but there are only a few studies that model the complex transient reaction of topography due to changes in uplift rate (if not stated differently, "uplift" means "rock uplift" herein) (e.g., Braun and van der Beek, 2004; Fox et al., 2014a). Depending on the boundary conditions (e.g., erosional coefficient, length of drainage system), transferring uplift signals through the entire landscape requires as much as millions of years (e.g., Whipple, 2001). A single uplift pulse results in an erosional upstream-migrating wave, which may be misinterpreted as a long-lasting or migrating uplift event if the transient evolution of landscape is not taken into account. A potential method to prevent such misinterpretation and bridge analytical time scales is the analysis of river profiles (e.g., Pritchard et al., 2009). Rivers are dynamic systems that react to changes in tectonic uplift and climate conditions, which may be recorded as distinct knickpoints in river profiles. An increasing number of studies have inverted river profiles to estimate uplift histories (e.g., Roberts and White, 2010; Fox et al., 2014b; Paul et al., 2014). These studies have incorporated analytical data to calibrate erosional models, but their inversions are driven solely by river profiles. In this study, I take a step forward and invert river profiles and analytical data (cosmogenic nuclide and thermochronological data) simultaneously.

MODELING APPROACH

This study, for the first time, presents a fully coupled landscape evolution modeling (LEM) approach that simultaneously fits river profiles and independent analytical data that quantify short- to long-term Earth surface processes (Fig. 1). The major benefit of the presented modeling approach is the possibility to extract an uplift history that is consistent with (1) analytical data sensitive to different time scales, and (2) the shape of river profiles and thus topography. Previous approaches based on river profiles used independent geological data, including thermochronological and cosmogenic observations, to check the consistency between uplift histories derived from river inversion and to tune model

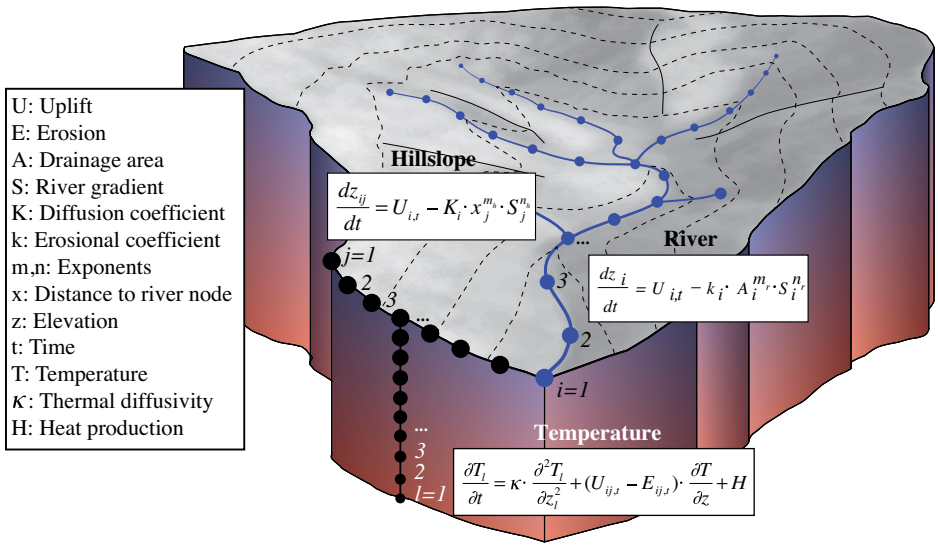

Figure 1. Principal model setup and equations. River evolution is modeled with a stream power equation, where drainage area is used to approximate discharge. Hillslope evolution is modeled assuming a slope-dependent erosion law, where *k* is assumed to be constant along the hillslope. Temperature evolution is modeled with the one-dimensional heat-transfer equation, and surface and basal temperatures are used as boundary conditions.

*E-mail: glotzbach@geowi.uni-hannover.de

parameterization (e.g., Paul et al., 2014). The philosophy of the presented integrated modeling approach is different; parameters controlling the pace of erosion, such as the erosional coefficient (k) and the exponents of discharge (m_r) and slope (n_r) in the stream power equation are free parameters during inversion (Fig. 1). Tuning of these parameters occurs during the inversion and evaluation of the fit between modeled and observed data. A corresponding program is implemented in MATLAB and consists of (1) a forward function that models river profiles and analytical data for a specified uplift history, and (2) an inversion routine that solves the forward problem with the objective of maximizing the fit between observation and model.

The program extracts the drainage system from a digital elevation model and calculates the river evolution at distinct river nodes with constant spacing using the stream power equation (e.g., Whipple and Tucker, 1999) (Fig. 1). Hillslopes are modeled with a constant length and spacing assuming a slope-dependent erosion law, a diffusion coefficient of 0.01 m/s, and exponents of distance (n_h) and slope (m_h) of 0 and 1 respectively (e.g., Kirkby, 1971), whereas the change in elevation of the connected river node is used as a boundary condition, and the maximum slope between hillslope nodes is limited to a critical hillslope (e.g., 30°). A standard finite-element technique is used to solve the stream power and hillslope equations, and the stability (uplift > erosion) is guaranteed by choosing an appropriate time step (<1 k.y.). The elevation, uplift, and erosion history of each river and hillslope node is recorded during modeling and used as input to calculate cosmogenic nuclide concentrations and thermochronological data. Cosmogenic nuclide concentrations are numerically integrated from great depth (several tens of meters) to the surface using depth- and latitude-dependent spallogenic (P_{sp}) and muonic (P_μ) production rates of Stone (2000) and Braucher et al. (2013):

$$N(z) = \left[N(z-1) + (P_{sp}[z] + P_\mu[z]) \cdot dt \right] \cdot e^{-\lambda \cdot dt}, \quad (1)$$

where $N(z)$ is the nuclide concentration at depth z, λ is the decay constant of ^{10}Be, and dt is the time step of the integration, which is 100 yr in all presented calculations. Note that z is the product of the site-specific erosion rate and the time step, and thus might vary from node to node. Catchment-wide ^{10}Be concentrations ($\bar{N}$) are calculated with:

$$\bar{N} = \frac{1}{n} \cdot \sum_{i=1}^{n} \left(E_{ij,t=0} \cdot N_{ij,z=0} \right), \quad (2)$$

where $E_{ij,t=0}$ is the erosion rate at node ij at model end, and $N_{ij,z=0}$ is the corresponding ^{10}Be concentration at the surface. At thermochronological sample locations, the 1-D heat-transfer equation is solved numerically with a finite-difference technique and standard thermal parameters (thermal diffusivity of 1×10^{-6} m^2/s, heat production of 9.6×10^{-10} W/kg, density of 2700 kg/m^3, specific heat capacity of 800 J/[kg K]). The heat production is temporally stable and decreases exponentially with depth, reaching 1/e of the surface production in 10 km depth. The upper thermal boundary is calculated with an atmospheric lapse rate of 5 °C/km, a sea-level temperature of 20 °C, and the site-specific elevation history of the thermochronological sample location. The basal thermal boundary is at 30 km depth for all models and calculated with an initial geothermal gradient (e.g., 20 °C/km, which yields 600 °C at 30 km depth). A stable geotherm is used as an initial condition, and the surface and basal temperatures are used as boundary conditions. Extracted time-temperature (tT) paths are used to calculate apatite (U-Th)/He and fission-track ages and track length distributions with the annealing and diffusion models of Farley (2000) and Ketcham et al. (1999). The fit between observed and modeled data drives a neighborhood algorithm inversion, which efficiently solves the inverse problem and extracts statistical parameters such as posterior marginal probability density functions of free parameters (see Section DR1 in the GSA Data Repository[1] for additional methodological details). The performance and sensitivity of the model was tested via inversion of two synthetically generated data sets consisting of river profile and thermochronological and cosmogenic nuclide data (Section DR2 in the Data Repository). The synthetic models converge to the correct solution, i.e., all free parameters are correctly predicted.

LANDSCAPE EVOLUTION OF THE SILA MASSIF

The presented data-driven inverse modeling is applied to reconstruct the landscape evolution of the Trionto river in the northern Sila massif in southern Italy (Fig. 2). This river basin was selected based on the following criteria: (1) availability of thermochronological data and sub-basin cosmogenic nuclide data (Olivetti et al., 2012; Vignaroli et al., 2012), (2) independent information about the uplift history from dated terraces (e.g., Robustelli et al., 2009), and (3) the visible absence of river captures and nearly identical χ values across drainage divides (Fig. 2B), indicating a near equilibrium of the river network and basin size (Willett et al., 2014). The Sila massif is a fault-bounded massif with a low-relief relict landscape at 1000–1600 m elevation separated by distinct river profile knickpoints from actively incising gorges at the massif flanks (Olivetti et al., 2012). The steepness of river segments and the position of knick-

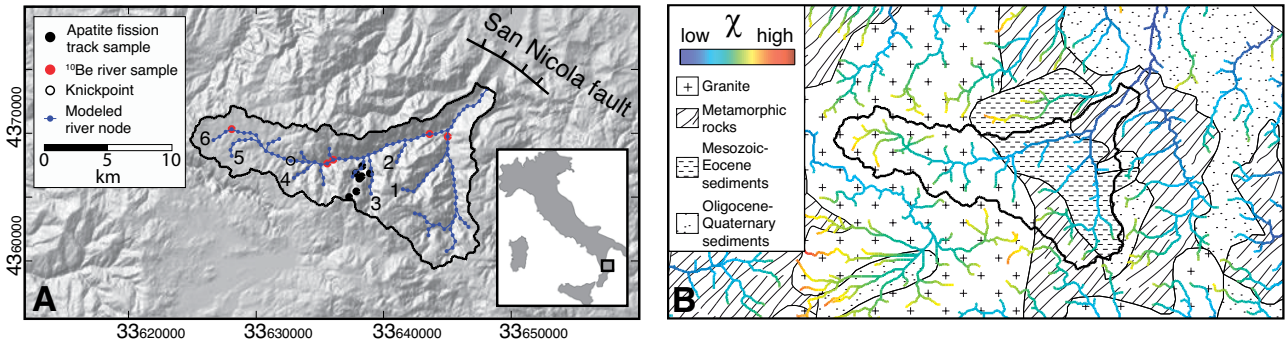

Figure 2. Topography, drainage network, and sample locations of northern Sila massif, southern Italy. A: Shaded relief (see location on inset map of Italy) with drainage network of Trionto river and published apatite fission-track (Vignaroli et al., 2012) and cosmogenic ^{10}Be sample locations (Olivetti et al., 2012). Some rivers are labeled with bold black numbers to facilitate locating them in Figure 3A. B: Lithological map with drainage network color coded with χvalue, which is a measure of the dynamic state of the river network (Willett et al., 2014).

[1]GSA Data Repository item 2015166, methodological details, performance testing of the model, inversion results of the Sila massif taking into account isostasy, and river profile evolution of the Trionto river, is available online at www.geosociety.org/pubs/ft2015.htm, or on request from editing@geosociety.org or Documents Secretary, GSA, P.O. Box 9140, Boulder, CO 80301, USA.

points are not controlled by lithology (Figs. 2B and 3A), suggesting that erodibilities of outcropping lithologies (granite, metamorphic rocks, and sediments) can be approximated and modeled with a single erosional coefficient.

The massif experienced a major exhumation pulse between 25 and 15 Ma (e.g., Vignaroli et al., 2012), followed by a phase of tectonic quiescence that may have led to the development of a low-relief landscape. Renewed uplift likely initiated not before the late Pliocene with rates of 0.6–1.0 mm/yr since 300–400 ka as recorded by early Pleistocene erosional debris and dated terraces (e.g., Westaway, 1993; Robustelli et al., 2009; Olivetti et al., 2012). The well-constrained uplift history of the Sila massif and available analytical data enable the performance of the numerical modeling approach to be tested and the local uplift history to be constrained. The inversion is based on the river profile of the Trionto river drainage system and available cosmogenic ^{10}Be and apatite fission-track data (Figs. 2 and 3A). 1-D marginals of the posterior probability distribution are more or less Gaussian (P4) or skewed (P2, P3, P5, P7, P8) distributed, whereas some pairs of parameters reveal clear trade-offs (Figs. 3B and 3C), such as the trade-off between exponent n_r and the concavity index (m_r/n_r). A good fit is obtained with an erosional coefficient of 5.0 ± 2.6 × 10^{-6}, an exponent n_r of 0.93 ± 0.16, a concavity index (m_r/n_r) of 0.47 ± 0.06, and a geothermal gradient of 28.7 ± 5.5 °C/km. According to the interpretation of the analytical data, a three-step uplift history was modeled. The inversion results suggest that the initial uplift occurred with a rate of 1.20 ± 0.45 km/m.y. and lasted until 15.7 ± 2.1 Ma (Fig. 3B). Afterward, uplift decreased to 0.09 ± 0.04 km/m.y. until 0.86 ± 0.44 Ma, and finally increased to 0.88 ± 0.44 km/m.y. The fast Miocene cooling recorded in the apatite fission-track data forces the inversion to predict fast uplift, which may have produced significant Miocene topography and relief. The succeeding slow uplift (0.09 ± 0.04 km/m.y.) is likely the consequence of isostatic compensation due to erosional unloading and the decay of topography. Taking into account the isostatic response to changes in topography, however, results in a comparable uplift history (P1: 16 ± 2.4 Ma; P2:1.05 ± 0.48 Ma; P3: 0.07 ± 0.06 km/m.y.; P4: 0.82 ± 0.43 km/m.y; see Section DR3 in the Data Repository).

The latter uplift rate derived for the hanging wall of the San Nicola fault excellently fits independent estimates derived from uplifted marine terraces in the footwall, suggesting that rapid uplift has occurred with ~1 km/m.y. at least since 300–400 ka (e.g., Robustelli et al., 2009). Therefore, negligible relative vertical movement has occurred along the fault since 300–400 ka. The exact timing and rate of the earlier uplift is not well constrained, but the inversion suggests that rapid uplift of the footwall may have initiated already in early Pleistocene times (Fig. 3B), in accordance with the transition from a shelf-type to a Gilbert-type fan delta in late early Pleistocene times in the Crati Basin bounding the Sila massif to the east and north (Colella, 1988). The estimated uplift fits well the timing of an overall change in the tectonic and magmatic setting in southern Italy (e.g., Westaway, 1993), and thus is likely related to deep-seated crustal or mantle changes (e.g., Gvirtzman and Nur, 2001). Assuming that rapid uplift continues in future times, the upstream river segments of the Trionto river will increase in elevation from ~1100 m at present to ~1700 m in 2 m.y. when they will reach a steady state (Section DR4 in the Data Repository).

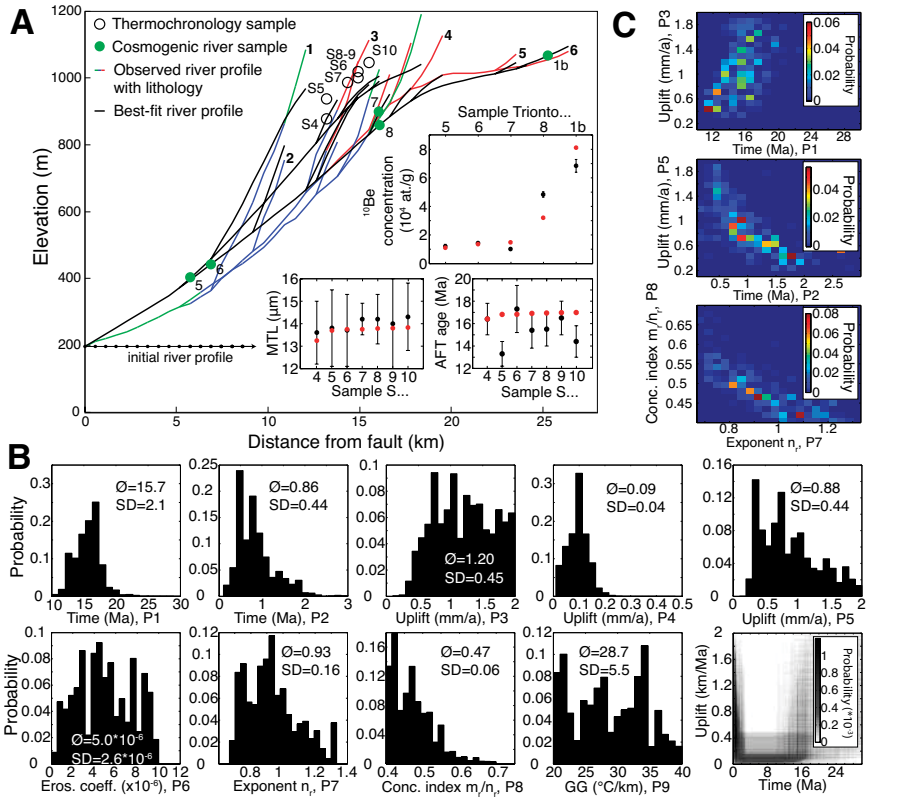

Figure 3. Results of inverse-modeled Trionto river (southern Italy) profile thermochronological and cosmogenic ^{10}Be data. A: Observed and best-fit river profile, apatite fission-track (AFT) age, mean apatite fission-track length (MTL), and cosmogenic ^{10}Be nuclide concentrations of sample localities. Observed river profile is color coded according to lithology (green, metamorphic rocks; blue, Mesozoic–Eocene sediments; red, granite). Black and red dots in the inset diagrams represent observed and modeled (best-fit) analytical data. Best-fit model yields normalized misfit of 18 for the following parameters (P1–P9): 15.8 Ma, 0.51 Ma, 1.36 mm/yr, 0.13 mm/yr, 1.74 mm/yr, 8.44 × 10^{-7}, 0.91, 0.64, and 23.0 °C/km. Some rivers are labeled with bold black numbers to facilitate locating them in Figure 2. B: One-dimensional marginal distributions of posterior probability distributions with their mean values (Ø) and standard deviations (SD). Note that limit of *x*-axis corresponds to the limit to which free parameters were allowed to vary. Lower right diagram shows two-dimensional marginal distribution of uplift history derived by combining parameters P1–P5. Eros.—erosion; Conc.—concentration; GG—geothermal gradient. C: Two-dimensional marginal distributions of posterior probability distribution of parameter pairs that show obvious trade-offs.

DISCUSSION AND CONCLUSIONS

The application of the integrated modeling approach to synthetic and natural data sets demonstrates its functionality and performance, especially the ability to resolve precise and accurate uplift histories. In the case of the Sila massif, the uplift is mainly regional, but part of it is accommodated along distinct fault segments (e.g., Westaway, 1993). Comparing the inversion-derived uplift rate for the Sila massif in the footwall of the San Nicola fault (0.88 ± 0.44 km/m.y.) with that derived from uplifted marine terraces in the hanging wall (1.0 ± 0.1 km/m.y.) suggests that only minor relative uplift, if any, occurs by footwall uplift. Thus the presented approach may also be applied to quantify the timing and pace of vertical fault movements that are otherwise difficult to determine. I further envision that the increasing amount of available analytical data will make the presented approach widely applicable to many fluvial landscape environments. Resulting uplift histories can be used to study the coupling between tectonics, climate, and Earth's surface processes

in the past and to predict how Earth's surface may respond to such change in the future.

ACKNOWLEDGMENTS

I thank A. Hampel and R. Hetzel for discussion and comments on an earlier version of the manuscript. Helpful comments and suggestions by Matthew Fox, Gareth Roberts, and two anonymous reviewers greatly improved the original manuscript.

REFERENCES CITED

Braucher, R., et al., 2013, Determination of muon attenuation lengths in depth profiles from in situ produced cosmogenic nuclides: Nuclear Instruments & Methods in Physics Research: Section B, Beam Interactions with Materials and Atoms, v. 294, p. 484–490, doi:10.1016/j.nimb.2012.05.023.

Braun, J., and van der Beek, P., 2004, Evolution of passive margin escarpments: What can we learn from low-T thermochronology?: Journal of Geophysical Research, v. 109, F04009, doi:10.1029/2004JF000147.

Braun, J., van der Beek, P., Valla, P., Robert, X., Herman, F., Glotzbach, C., Pedersen, V., Perry, C., Simon-Labric, T., and Prigent, C., 2012, Quantifying rates of landscape evolution and tectonic processes by thermochronology and numerical modeling of crustal heat transport using PECUBE: Tectonophysics, v. 524–525, p. 1–28, doi:10.1016/j.tecto.2011.12.035.

Buscher, J.T., Hampel, A., Hetzel, R., Dunkl, I., Glotzbach, C., Struffert, A., Akal, C., and Rätz, M., 2013, Quantifying rates of detachment faulting and erosion in the central Menderes Massif (western Turkey) by thermochronology and cosmogenic ^{10}Be: Journal of the Geological Society, v. 170, p. 669–683, doi:10.1144/jgs2012-132.

Colella, A., 1988, Fault-controlled marine Gilbert-type fan deltas: Geology, v. 16, p. 1031–1034, doi:10.1130/0091-7613(1988)016<1031:FCMGTF>2.3.CO;2.

England, P., and Molnar, P., 1990, Surface uplift, uplift of rocks, and exhumation of rocks: Geology, v. 18, p. 1173–1177, doi:10.1130/0091-7613(1990)018<1173:SUUORA>2.3.CO;2.

Farley, K.A., 2000, Helium diffusion from apatite: General behavior as illustrated by Durango fluorapatite: Journal of Geophysical Research, v. 105, p. 2903–2914, doi:10.1029/1999JB900348.

Fox, M., Reverman, R., Herman, F., Fellin, M.G., Sternai, P., and Willett, S.D., 2014a, Rock uplift and erosion rate history of the Bergell intrusion from the inversion of low temperature thermochronometric data: Geochemistry Geophysics Geosystems, v. 15, p. 1235–1257, doi:10.1002/2013GC005224.

Fox, M., Goren, L., May, D.A., and Willett, S.D., 2014b, Inversion of fluvial channels for paleorock uplift rates in Taiwan: Journal of Geophysical Research, v. 119, p. 1853–1875, doi:10.1002/2014JF003196.

Glotzbach, C., van der Beek, P., Carcaillet, J., and Delunel, R., 2013, Deciphering the driving forces of erosion rates on millennial and million-year timescales in glacially impacted landscapes: An example from the Western Alps: Journal of Geophysical Research, v. 118, p. 1491–1515, doi:10.1002/jgrf.20107.

Gvirtzman, Z., and Nur, A., 2001, Residual topography, lithospheric structure and sunken slabs in the central Mediterranean: Earth and Planetary Science Letters, v. 187, p. 117–130, doi:10.1016/S0012-821X(01)00272-2.

Ketcham, R.A., Donelick, R.A., and Carlson, W.D., 1999, Variability of apatite fission-track annealing kinetics: III. Extrapolation to geological time scales: The American Mineralogist, v. 84, p. 1235–1255.

Kirkby, M.J., 1971, Hillslope process-response models based on the continuity equation, *in* Brunsden, D., ed., Slopes: Form and Process: Institute of British Geographers Special Publication 3, p. 15–30.

Maher, K., and Chamberlain, C.P., 2014, Hydrologic regulation of chemical weathering and the geologic carbon cycle: Science, v. 343, p. 1502–1504, doi:10.1126/science.1250770.

National Research Council, 2010, Landscapes on the Edge: New Horizons for Research on Earth's Surface: Washington, D.C., The National Academies Press, 180 p.

Olivetti, V., Cyr, A.I., Molin, P., Faccenna, C., and Granger, D.E., 2012, Uplift history of the Sila Massif, southern Italy, deciphered from cosmogenic ^{10}Be erosion rates and river longitudinal profile analysis: Tectonics, v. 31, TC3007, doi:10.1029/2011TC003037.

Paul, J.D., Roberts, G.G., and White, N., 2014, The African landscape through space and time: Tectonics, v. 33, p. 898–935, doi:10.1002/2013TC003479.

Pritchard, D., Roberts, G.G., White, N.J., and Richardson, C.N., 2009, Uplift histories from river profiles: Geophysical Research Letters, v. 36, L24301, doi:10.1029/2009GL040928.

Raymo, M.E., and Ruddiman, W.F., 1992, Tectonic forcing of late Cenozoic climate: Nature, v. 359, p. 117–122, doi:10.1038/359117a0.

Reiners, P.W., and Ehlers, T.A., eds., 2005, Low-Temperature Thermochronology: Techniques, Interpretations, and Applications: Reviews in Mineralogy and Geochemistry, v. 58, 622 p.

Roberts, G.G., and White, N., 2010, Estimating uplift rates histories from river profiles using African examples: Journal of Geophysical Research, v. 115, B02406, doi:10.1029/2009JB006692.

Robustelli, G., Lucà, F., Corbi, F., Pelle, T., Dramis, F., Fubelli, G., Scarciglia, F., Muto, F., and Cugliari, D., 2009, Alluvial terraces on the Ionian coast of northern Calabria, southern Italy: Implications for tectonic and sea level controls: Geomorphology, v. 106, p. 165–179, doi:10.1016/j.geomorph.2008.12.010.

Stone, J., 2000, Air pressure and cosmogenic isotope production: Journal of Geophysical Research, v. 105, p. 23,753–23,759, doi:10.1029/2000JB900181.

Vignaroli, G., Minelli, L., Rossetti, R., Balestrieri, M.L., and Faccenna, C., 2012, Miocene thrusting in the eastern Sila massif: Implications for the evolution of the Calabria-Peloritani orogenic wedge (southern Italy): Tectonophysics, v. 538–540, p. 105–119, doi:10.1016/j.tecto.2012.03.011.

von Blanckenburg, F., 2005, The control mechanisms of erosion and weathering at basin scale from cosmogenic nuclides in river sediment: Earth and Planetary Science Letters, v. 237, p. 462–479, doi:10.1016/j.epsl.2005.06.030.

West, A.J., 2012, Thickness of the chemical weathering zone and implications for erosional and climatic drivers of weathering and for carbon-cycle feedbacks: Geology, v. 40, p. 811–814, doi:10.1130/G33041.1.

Westaway, R., 1993, Quaternary uplift of southern Italy: Journal of Geophysical Research, v. 98, p. 21,741–21,772, doi:10.1029/93JB01566.

Whipple, K.X, 2001, Fluvial landscape response time: How plausible is steady-state denudation?: American Journal of Science, v. 301, p. 313–325, doi:10.2475/ajs.301.4-5.313.

Whipple, K.X, and Tucker, G.E., 1999, Dynamics of the stream-power river incision model: Implications for height limits of mountain ranges, landscape response timescales, and research needs: Journal of Geophysical Research, v. 104, p. 17,661–17,674, doi:10.1029/1999JB900120.

Willett, S.D., McCoy, S.W., Perron, J.T., Goren, L., and Chen, C.-Y., 2014, Dynamic reorganization of river basins: Science, v. 343, 1248765, doi:10.1126/science.1248765.

Manuscript received 11 February 2015
Revised manuscript received 26 February 2015
Manuscript accepted 3 March 2015

Printed in USA